ARTICLE

Threshold Photoelectron Spectrum of CF_2Cl_2 in Photon Energy Range of 13.9–15.1 eV†

Baokun Shan[a‡], Xinlang Yang[a‡], Tongpo Yu[b,c*], Yan Chen[a], Ning Zhang[a], Xiaoguo Zhou[a*], Shilin Liu[a*]

a. Department of Chemical Physics, University of Science and Technology of China, Hefei 230026, China
b. Department of Physics, Hefei University of Technology, Hefei 230009, China
c. National Synchrotron Radiation Laboratory, University of Science and Technology of China, Hefei 230029, China

(Dated: Received on August 22, 2023; Accepted on September 26, 2023)

Threshold photoelectron spectroscopy of dichlorodifluoromethane (CF_2Cl_2) has been re-investigated using a combination of photoelectron-photoion coincidence measurement and density functional theory calculations. For the D^2B_2 band of threshold photoionization spectra in the energy range of 13.9– 15.1 eV, a series vibrational peaks were clearly observed. Using the optimized geometries and vibrational frequencies of the CF_2Cl_2 neutral and its cations in the D^2B_2 ionic state at the M06-2X/aug-cc-pVTZ level of theory, Franck-Condon factor simulations were carried out, and showed perfect agreement with the experimental spectra. Accordingly, the satisfactory vibrational assignments for the D^2B_2 band were achieved, and the adiabatic and vertical ionization energies to the D^2B_2 ionic state were determined as 14.125±0.005 eV and 14.355 ± 0.005 eV, respectively. Moreover, vibrational frequencies of the ν_1^+ and ν_3^+ modes were 1178 cm^{-1} and 361 cm^{-1}, respectively, as well as the anharmonic parameter for the ν_3^+ mode of 3.42 cm^{-1}.

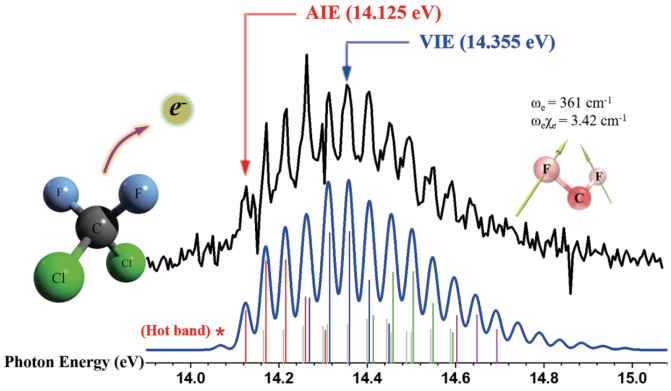

Key words: CF_2Cl_2, Photoelectron spectroscopy, Vibrational spectroscopy, Photoionization, Coincidence

I. INTRODUCTION

Dichlorodifluoromethane (CF_2Cl_2), a typical representative of Freons, is an important chemical in industries of refrigerant, aerosol propellant, and plasma processing agent [1–4]. Its close connection with the extensive destruction of the ozone layer has attracted extensive attentions, as its unimolecular decomposition can release reactive chlorine atoms when absorbing solar ultra-violet (UV) light [5, 6]. Therefore, accurate ionization energies (IEs) and dissociation dynamics of CF_2Cl_2 are crucial for an insight into the atmospheric chemistry of fluorocarbons [7–11].

Generally, significant variation of molecular geometry and highly vibrational excitation in photoionization

† Part of Special Issue "In Memory of Prof. Qihe Zhu on the occasion of his 100th Aniversary".
‡ These authors contributed equally to this work.
* Authors to whom correspondence should be addressed. E-mail: topoyu@hfut.edu.cn, xzhou@ustc.edu.cn, slliu@ustc.edu.cn

may lead to that the 0-0 vibrational band of photoelectron spectra (PES) or threshold photoelectron spectra (TPES) has relatively weak intensity. In this circumstance, the identification of adiabatic ionization energy (AIE) is relatively difficult according to the Franck-Condon principle [12–15]. Therefore, there were some controversies of the AIE value in previous experiments and theoretical calculations. According to the AIE definition as the 0-0 band origin in experimental spectra, a correct vibrational assignment is essentially pivotal to determine the AIE values, and illuminates reasonably the previous disagreement. Therefore, by using the Franck-Condon simulation with the calculated vibrational frequencies, we have obtained prefect spectral assignments for the vibrationally resolved TPES of CF_2Cl_2 in the X^2B_2 [16], B^2B_1, and C^2A_1 ionic states [17], and then the corresponding AIE values of these ionic states have been corrected. For example, the AIE of CF_2Cl_2 towards the X^2B_2 ground ionic state is realigned to be 11.565 ± 0.010 eV [16], which is much lower than the spectral onset of ~11.75 eV.

In comparison to these lower electronic states, vibrationally resolved PES [18–22] and threshold PES (TPES) [11, 16, 17] were experimentally measured previously for the D^2B_2 ionic state in the photon energy range of 13.9–15.0 eV. Jadrny *et al.* [21] observed a series of vibrational peaks with a space of ~46 meV (371 cm^{-1}) and attributed them to the excitation of the ν_3^+ vibrational mode, resulting in an AIE value of 14.123 eV from the lowest-energy peak position. Using the identical approach, Pradeep and Shirley [22] reported the ν_3^+ frequency of 375 cm^{-1}, the anharmonicity coefficient $\omega_e\chi_e$ of 0.27 cm^{-1}, and the AIE value of 14.126 eV. Cvitas [20] and Bunzli [18] suggested the ν_3^+ frequency to be 360 cm^{-1} and 370±40 cm^{-1}, respectively. Notably, these vibrational assignments were obtained simply according to the energy interval of vibrational peaks. Thus, these conclusion could have relatively large uncertainties inevitably, and even might lead to errors in the absence of high-level theoretical calculations. It gave us a motivation to re-investigate the TPES of CF_2Cl_2 in the D^2B_2 state, using the combination of experimental measurements and quantum chemical calculations.

In this work, we measured the TPES of CF_2Cl_2 in the D^2B_2 state using the threshold photoelectron-photoion coincidence (TPEPICO) double velocity map imaging apparatus at the Hefei Light Source [23]. The photon energies in the whole range of 11.60–15.10 eV were charily calibrated by comparing with the absorption lines of argon atoms. For the D^2B_2 state, we carried out quantum chemical calculations for optimized geometries and vibrational frequencies of the neutral CF_2Cl_2 molecule in ground state and its cationic D^2B_2 state at various levels of theory. By performing Franck-Condon factor simulations on the experimental spectra, the vibrational structure of the D^2B_2 state was perfectly reproduced, providing the great spectral assignments. Consequently, the accurate AIE values towards the D^2B_2 state were determined reliably. In addition, the comparison between the current experimental spectra and quantum chemical calculation results also provided significant feedbacks on the reliability of the theoretical levels.

II. EXPERIMENTAL AND COMPUTATIONAL METHODS

The experiments were conducted at the BL09U beamline at the National Synchrotron Radiation Laboratory in Hefei, China. Only brief introductions were given here as the synchrotron beamline and the TPEPICO velocity imaging spectrometer were described in detail in Ref.[23]. Vacuum ultra-violet (VUV) photons in the range of 11.60–15.10 eV were emitted from the undulator of an 800 MeV electron storage ring, and then were dispersed through a 6 m-long monochromator (370 grooves/mm). The energy resolution ($E/\Delta E$) was reported to be ~2000 [24]. A gas filter full of inert gases such as helium, neon or argon was placed in the front of the TPEPICO chamber, to eliminate more than 99% of high-order harmonic radiation. In the current experiments, argon gas was used. The photon fluxes were recorded with a silicon photodiode, for normalizing ion intensity from the radiation intensity.

A mixture gas of CF_2Cl_2 and helium (1/9, v/v) with a stagnation pressure of 1.2 atm was introduced into the vacuum chamber through a 20-μm-diameter nozzle. The continuous supersonic beam was collimated with a 0.5-mm-diameter skimmer, and intersected with the VUV photons at approximately 10 cm downstream. In photoionization, the produced electrons and ions were extracted in opposite directions with the direct-current (DC) electric field of 15 V/cm. With the action of ion optics, all photoelectrons with zero kinetic energy (so-called threshold photoelectrons) produced in the ioniza-

DOI: 10.1063/1674-0068/cjcp2308074

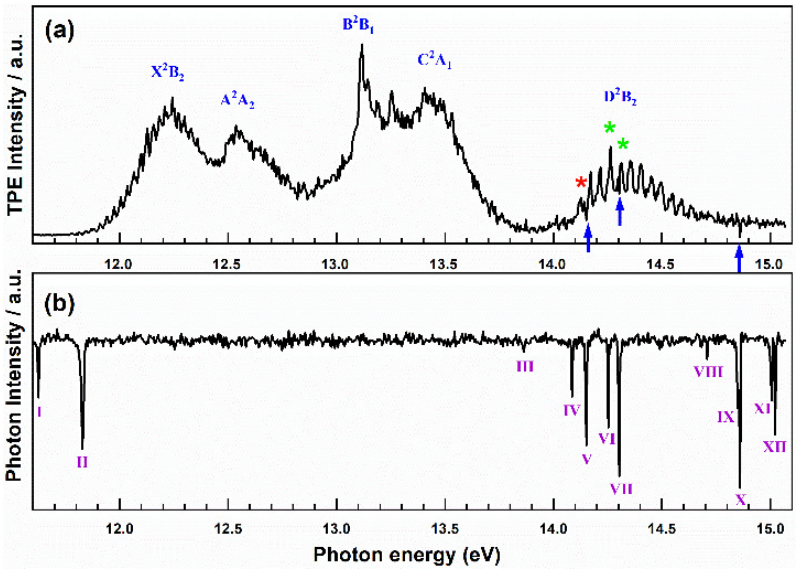

FIG. 1 (a) Threshold photoelectron spectrum of CF_2Cl_2 in the photon-energy range of 11.60–15.10 eV with the step size of 5 meV, where a red star and two green stars marked the first vibrational peak and the strongest vibronic band of the D^2B_2 state, respectively, and three blue arrows marked three sharp indentations. (b) Photon flux of the VUV synchrotron radiation, simultaneously measured in experiments, in which a series of sharp, negative peaks I–XII were observed.

tion zone could be velocity-focused into an 1-mm-diameter aperture on the mask at the end of the electron flight tube, while the "hot" electrons with velocity components vertical to the flight axis were velocity-mapped onto surrounding concentric rings on the mask. Thus, the "pure" TPES could be obtained by subtracting this contamination of the "hot" electrons as described previously [25, 26]. Time-of-flight (TOF) measurements of ions were triggered by the photoelectrons, and the single-start multi-stop data acquisition mode was used in our coincidence experiments [27]. Using the TPEPICO approach, the photoionization and dissociative photoionization of several molecules have been successfully investigated [28–31].

To get reliable assignments of the TPES of CF_2Cl_2 in the D^2B_2 state, we calculated the optimized geometries and harmonic vibrational frequencies of the $CF_2Cl_2(X^1A_1)$ and $CF_2Cl_2^+(D^2B_2)$ using density functional theory (DFT) and time-dependent DFT (TD-DFT), respectively. The M06-2X [32] level of theory with the aug-cc-pVTZ basis set was chosen in current calculations. The results were compared with the previous data at the other theoretical levels, such as HF [33], MRCI [34], CASSCF and CASPT2 [35], to assess the reliability of computations. Notably, as proposed previously [16, 17], the ωB97XD [36] approach was effective for the X^2B_2, B^2B_1, and C^2A_1 ionic states among all common DFT levels, due to the more significant contribution of the HF component. As shown in Section III.C, the M06-2X shows better performances for the D^2B_2 state than the ωB97XD method. Using the calculated geometries, the vibrational frequencies, and vectors, the Franck-Condon factor was calculated using the ezSpectrum software [37], as the overlap integral of the vibrational wavefunctions between the initial and target states. The vibrational temperature of 250 K and a full width at half maximum (FWHM) of 25 meV were used in the simulations. All these quantum chemical calculations were carried out with the Gaussian 16 C.01 package [38].

III. RESULTS AND DISCUSSION

A. Threshold photoelectron spectrum of CF_2Cl_2

FIG. 1(a) shows the TPES of CF_2Cl_2 in the range of 11.60–15.10 eV with the step size of 5 meV. Five electronic states were involved as X^2B_2, A^2A_2, B^2B_1, C^2A_1, and D^2B_2, consistent with previous He-I photoelectron spectra [18, 20–22]. A series of vibrational peaks were more clearly observed in the D^2B_2 band, compared to the lower electronic states. Its first peak with a red star was located at 14.125 eV, in general line with the previous experimental conclusions [21, 22]. Actually, this peak was consistently assigned to the 0-0 band in the experiments. Moreover, the vibrational peak with the strongest intensity was located at 14.260 eV, which is

DOI: 10.1063/1674-0068/cjcp2308074

TABLE I Experimental and referenced absorption lines of argon gas (ΔE=$E_{\text{Expt.}}$–$E_{\text{Ref.}}$). Peaks are labeled in FIG. 1.

Peak	Position/eV		ΔE/eV	Lower Level(Conf., Term, J)	Upper Level(Conf., Term, J)
	$E_{\text{Expt.}}$	$E_{\text{Ref.}}$ [39]			
I	11.625	11.623	0.002	$3s^23p^6$, ^{1}s, 0	$3s^23p^5(^2P^0_{3/2})4s$, $^2[3/2]^0$, 1
II	11.828	11.828	0.000	$3s^23p^6$, ^{1}s, 0	$3s^23p^5(^2P^0_{1/2})4s$, $^2[1/2]^0$, 1
III	13.863	13.863	0.000	$3s^23p^6$, ^{1}s, 0	$3s^23p^5(^2P^0_{3/2})3d$, $^2[1/2]^0$, 1
IV	14.086	14.090	−0.004	$3s^23p^6$, ^{1}s, 0	$3s^23p^5(^2P^0_{3/2})5s$, $^2[3/2]^0$, 1
V	14.151	14.152	−0.001	$3s^23p^6$, ^{1}s, 0	$3s^23p^5(^2P^0_{3/2})3d$, $^2[3/2]^0$, 1
VI	14.253	14.255	−0.002	$3s^23p^6$, ^{1}s, 0	$3s^23p^5(^2P^0_{1/2})5s$, $^2[1/2]^0$, 1
VII	14.303	14.303	0.000	$3s^23p^6$, ^{1}s, 0	$3s^23p^5(^2P^0_{1/2})3d$, $^2[3/2]^0$, 1
VIII	14.708	14.711	−0.003		
IX	14.850	14.848	0.002		
X	14.860	14.859	0.001		
XI	15.007	15.003	0.004		
XII	15.022	15.022	0.000		

TABLE II Vertical ionization energies (VIEs) and adiabatic ionization energies (AIEs) of CF_2Cl_2 reported in PES and TPES experiments.

Reference	Method	VIE/eV					AIE/eV			
		X^2B_2	A^2A_2	B^2B_1	C^2A_1	D^2B_2	X^2B_2	B^2B_1	C^2A_1	D^2B_2
Turner *et al.* [19]	PES	12.3	12.6	13.2	13.5	14.4				
Bunzli *et al.* [18]	PES	12.27	12.55	13.13	13.46	14.37				
Cvitas *et al.* [20]	PES	12.26	12.53	13.11	13.45	14.36				
Jadrny *et al.* [21]	PES	12.24	12.54	13.120	13.47	14.353		13.120		14.123
Pradeep *et al.* [22]	PES					11.734		13.078		14.126
Seccombe *et al.* [11]	TPES	12.28	12.55	13.14	13.45	14.41				
Our previous work [16, 17]	TPES	12.250	12.550	13.150	13.450		11.565	13.150	13.340	
This work	TPES	12.245	12.535	13.120	13.410	14.355	11.590	13.120	13.300	14.125

usually defined as the vertical ionization energy (VIE). In addition, three sharp indentations (marked with blue arrows in FIG. 1(a)) were observed within the D^2B_2 band. It is worth noting that their energy positions exactly agreed with the V, VII, and X peaks in FIG. 1(b).

As the gas filter full of argon gas was used in current experiments to eliminate high-order harmonic radiation, the absorption of argon atoms caused significant decrease in the VUV flux. As shown by the VUV photon flux of the synchrotron radiation in FIG. 1(b), a series of sharp, negative peaks I– XII were observed indeed, providing a perfect wavelength calibration for the experimental photon energy. Table I lists the calibrated energy positions and the argon atomic absorption lines in the database [39]. The differences between the experimental and referenced peak positions are less than ±4 meV and within the uncertainty of the current VUV photon energies. It is worth noting that in our previous experiments of $CF_2Cl_2^+$ in the X^2B_2, A^2A_2, B^2B_1, and C^2A_1 states [16, 17], only two absorption lines, I and II, of the argon gas could be observed below 14 eV, and both of them were located at the low-energy side of the X^2B_2 band (in FIG. 1(a)). Thus, the previous calibration might be insufficiently reliable for these states. Using the twelve absorption lines of argon in the whole energy range, we re-calibrated the VUV wavelength of the TPES and re-performed the Franck-Condon simulation for the X^2B_2, B^2B_1, and C^2A_1 bands as done previously using the reported vibrational frequencies.

The corrected VIE and AIE values of the X^2B_2, B^2B_1, and C^2A_1 ionic states are summarized in Table II, as well as the VIE value of the A^2A_2 state. For comparison, the previously reported data from the PES and TPES experiments are listed too [11, 18–22]. For example, the AIE value of CF_2Cl_2 towards the X^2B_2 state is

DOI: 10.1063/1674-0068/cjcp2308074

TABLE III Structural parameters of neutral CF_2Cl_2 molecule and $CF_2Cl_2^+$ cation in the D^2B_2 state. Bond length R in unit of Å and bond angle Θ in unit of (°)).

Method	CF_2Cl_2 (X^1A_1)				$CF_2Cl_2^+$ (D^2B_2)			
	R(C–F)	R(C–Cl)	Θ(F–C–F)	Θ(Cl–C–Cl)	R(C–F)	R(C–Cl)	Θ(F–C–F)	Θ(Cl–C–Cl)
ωB97XD	1.325	1.770	108.2	111.4	1.274	1.852	113.5	107.1
M06-2X	1.328	1.760	107.8	111.8	1.262	1.888	113.9	105.9
HF [33]	1.309	1.759	108.0	111.7				
CASSCF [35]					1.243	1.933	113.8	105.3
CASPT2 [35]	1.330	1.755	108.0	111.7	1.266	1.893	115.9	102.9

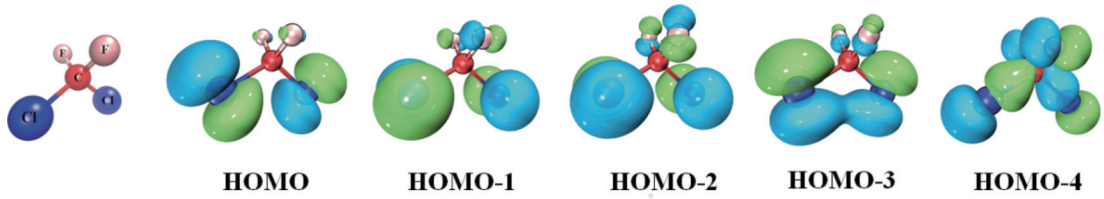

FIG. 2 The HOMO, HOMO-1, HOMO-2, HOMO-3, and HOMO-4 orbitals of neutral CF_2Cl_2.

corrected to be 11.590 eV from 11.565 eV in the literature [16], and the appearance energy, $AP(CF_2Cl^+/CF_2Cl_2)$, is revised from 11.945 eV [16] to 11.974 eV. Then, the C–Cl bond energy of $CF_2Cl_2^+$ cation can be calculated as BE(C–Cl in $CF_2Cl_2^+$) = $AP(CF_2Cl^+/CF_2Cl_2)$– AIE(CF_2Cl_2) = 0.384 eV. Notably, this value agrees well with the previous one of 0.380 ± 0.010 eV [16], due to the error canceling effect. In addition, two peaks of the D^2B_2 state at 14.263 eV and 14.313 eV with green stars in FIG. 1(a) have comparable intensities, according to the influence of the argon absorption line VII. Accordingly, it is not easy to directly identify the VIE value in absence of the Franck-Condon simulation.

B. Geometry and vibrational frequencies of $CF_2Cl_2^+$ in the D^2B_2 state

To perform the Franck-Condon simulation of the D^2B_2 band in FIG. 1(a), the optimized geometry and harmonic vibrational frequencies of D^2B_2 are necessary. Considering that the contribution of diffuse functions might be more significant in higher electronically excited states, we utilized the ωB97XD/aug-cc-pVTZ and M06-2X/aug-cc-pVTZ levels to calculate the property of the D^2B_2 state, since the reliability of the former was confirmed in our previous works [16, 17] and the latter usually has better performance owing to more contributions of HF components [32]. Similar to the low-lying states, CF_2Cl_2 remains C_{2v} symmetry in the Franck-Condon photoionization to the D^2B_2 state. Table III summarizes the optimized geometrical parameters of the neutral CF_2Cl_2 molecule and the $CF_2Cl_2^+$ cations in the D^2B_2 state at the two levels of theory, as well as the previous ones using the HF/MIDI-4 [33], CASPT2/ANO-L, and CASSCF/ANO-L methods [35]. All calculated results are generally consistent. The reduced C–F bond length and the elongated C–Cl bond are expected in photoionization. Moreover, at the M06-2X level, the Θ(F–C–F) angle is increased from 107.8° in neutral to 113.9° in the D^2B_2 ionic state, while Θ(Cl–C–Cl) decreases from 111.8° to 105.9°. These changes in bond angles indicate that the ionization of $CF_2Cl_2(X^1A_1) \rightarrow CF_2Cl_2^+(D^2B_2)$ would mainly accompany with the excitation of the scissor vibrations of the CF_2 or CCl_2 groups.

As shown in FIG. 2, we also calculated the five highest occupied molecular orbitals of the neutral CF_2Cl_2 molecule. Notably, the first four molecular orbitals are mainly contributed by the lone pair of electrons of the Cl atom and contain almost non-bonding orbitals, which is in line with Bunzli's conclusion [18]. In comparison, the D^2B_2 ionic state is formed by removing an electron from the HOMO-4 orbital, which is jointly contributed by the lone pair of electrons of the F atom and the σ(C–Cl) bonds. This complex orbital distribution implies that the molecular geometry might be significantly changed when forming the D^2B_2 state.

According to transition selection rules, only four vibrational modes of a_1 symmetry can be excited in the FC ionization, ν_1^+ to ν_4^+ for $CF_2Cl_2^+$ [21, 22, 33]. As described previously [16, 17], the ν_1^+ and ν_2^+ modes are mainly attributed to the motion of the carbon atom

DOI: 10.1063/1674-0068/cjcp2308074

TABLE IV Vibrational frequencies (cm^{-1}) of the four vibrational modes with a_1 symmetry for the D^2B_2 state of $CF_2Cl_2^+$ cations, at different quantum chemical levels of theory, comparing to the experimental data.

Method	ν_1^+	ν_2^+	ν_3^+	ν_4^+
Theor.				
ωB97XD	1168	677	401	229
M06-2X	1255	673	359	222
CASSCF [35]	1350	707	354	212
Expt.				
Pradeep *et al*. [22]	–	–	375	–
Bunzli *et al*. [18]	–	–	370±40	–
Cvitas *et al*. [20]	–	–	360	–
Jadrny *et al*. [21]	–	–	371	–
Turner *et al*. [19]	–	–	385	–
This work	1178	–	361	–

along the C_{2V} symmetry axis, combining with the C–F bond symmetry stretching and the F–C–F scissoring, respectively. The ν_3^+ mode is a combination of the C–Cl stretching and the F–C–F scissoring, while the ν_4^+ mode is contributed by the Cl–C–Cl scissoring. Table IV summarizes their vibrational frequencies calculated at different theoretical levels of theory and the experimental values. We note, in the previous experiments the distinct vibrational structure of the D^2B_2 band was consistently assigned to the ν_3^+ excitation, and the value of ~370 cm^{-1} was all suggested for its vibrational frequency [18–22]. In comparison to this value, the M06-2X and CASSCF frequencies are slightly lower, while the ν_3^+ frequency of 401 cm^{-1} at the ωB97XD level is apparently larger. However, the calculated results at three levels are generally consistent with each other. In this scenario, it is almost impossible to identify the best DFT approaches for the title system, without the Franck-Condon simulation for the whole spectral band.

C. Franck-Condon factor simulated TPE spectra

The FC factors (FCFs) usually can be expressed as the square of nuclear overlap terms, as $f_{i\to j} = |\langle\psi^*_{nuc,f}|\psi_{nuc,i}\rangle|^2$, where $\psi^*_{nuc,f}$ and $\psi_{nuc,i}$ are the nuclear wave functions of final and initial states. For the $CF_2Cl_2(X^1A_1)\to CF_2Cl_2^+(D^2B_2)$ photoionization, FCFs were calculated at the M06-2X and ωB97XD levels with the aug-cc-pVTZ basis set within harmonic oscillator model, using their own optimized geometries and vibrational frequencies of neutral and cationic molecules. The maximal vibrational quantum number of the neutral in ground state was set to be 5, whereby hot band excitations were considered too. Following the previous simulations for lower electronic states [16, 17], the thermal temperature were set at 250 K owing to the identical experimental conditions. Actually, we also compared the simulated spectra at the range of 20– 300 K (not shown here), affirming this optimized temperature.

Table V lists the vibrational excitations with the transition intensity (*i.e.* FCFs) of more than 0.010 in the photoionization towards the D^2B_2 ionic state, calculated at the M06-2X/aug-cc-pVTZ level, where the calculated peak positions were slightly shifted according to systematic errors in the excitation energy calculation. As indicated in this table, the ν_1^+ and ν_3^+ vibrational modes, together with their combination, play dominant roles in the photoionization process, while the ν_2^+ and ν_4^+ excitations have minor contributions. Specifically, the major vibrational peaks can be assigned as the vibrational transition series of $X^1A_1(0, 0, 0, 0)\to D^2B_2(m, 0, n, 0)$ ($m=0, 1, 2, 3$; $n=1, 2, 3, 4$). Furthermore, the hot-band transition process of $X^1A_1(0, 0, 0, 1)\to D^2B_2(m, 0, n, 1)$ (m=0, 1, 2; n=1, 2) also exhibits considerable intensity.

FIG. 3 shows the experimental and simulated threshold photoelectron spectra. To our surprise, the simulated spectrum at the M06-2X level exhibits generally consistent vibrational structures with the experimental data, while the spectral patterns of the ωB97XD simulated spectra do show significant difference, even if we ignore the discrepancies of peak positions. The different performances are unexpected, since the optimized geometries at the ωB97XD level do not show striking discrepancies from the other theoretical levels like M06-2X as shown in Table III. Actually, the two DFT methods have some difference in the HF component for exchange-correlation energy, *e.g.* 54% in M06-2X, 22.2% for short-range and 100% for long-range in ωB97XD. Therefore, the current result shows a representative example that the HF component has sensitive influences on the ν_1^+ and ν_3^+ vibrational frequencies of the $CF_2Cl_2^+(D^2B_2)$ cation (Table IV), further resulting in different spectral patterns.

As shown in FIG. 3, the dominant vibrational structure of the D^2B_2 band can be reproduced by the FCF simulation at the M06-2X level. Thus, our results provide solid evidences that the combinations of multiple

DOI: 10.1063/1674-0068/cjcp2308074

TABLE V Vibrational peak positions, Frank-Condon factors (FCFs), and corresponding transitions of the calculated threshold photoelectron spectrum of CF_2Cl_2 within the ionization energy range towards the D^2B_2 ionic state at the M06-2X/aug-cc-pVTZ level.

Peak position/eV	$\langle\psi^*_{\mathrm{nuc,f}}\|\psi_{\mathrm{nuc,i}}\rangle$	FCF	$X^1A_1(\nu_{1-4}) \rightarrow D^2B_2\ (\nu_{1-4}{}^+)$
14.125	0.153	0.023	(0,0,0,0)→(0,0,0,0)
14.165	−0.227	0.012	(0,0,0,1)→(0,0,1,1)
14.170	−0.230	0.053	(0,0,0,0)→(0,0,1,0)
14.210	0.229	0.012	(0,0,0,1)→(0,0,2,1)
14.215	0.232	0.054	(0,0,0,0)→(0,0,2,0)
14.255	0.118	0.014	(0,0,0,0)→(0,1,1,0)
14.260	−0.178	0.032	(0,0,0,0)→(0,0,3,0)
14.283	−0.175	0.031	(0,0,0,0)→(1,0,0,0)
14.300	−0.119	0.014	(0,0,0,0)→(0,1,2,0)
14.305	0.108	0.012	(0,0,0,0)→(0,0,4,0)
14.323	0.261	0.015	(0,0,0,1)→(1,0,1,1)
14.328	0.264	0.070	(0,0,0,0)→(1,0,1,0)
14.368	−0.262	0.015	(0,0,0,1)→(1,0,2,1)
14.373	−0.266	0.071	(0,0,0,0)→(1,0,2,0)
14.412	−0.136	0.018	(0,0,0,0)→(1,1,1,0)
14.418	0.204	0.042	(0,0,0,0)→(1,0,3,0)
14.440	0.147	0.022	(0,0,0,0)→(2,0,0,0)
14.457	0.137	0.019	(0,0,0,0)→(1,1,2,0)
14.463	−0.124	0.015	(0,0,0,0)→(1,0,4,0)
14.480	−0.219	0.011	(0,0,0,1)→(2,0,1,1)
14.485	−0.222	0.049	(0,0,0,0)→(2,0,1,0)
14.502	−0.105	0.011	(0,0,0,0)→(1,1,3,0)
14.525	0.220	0.011	(0,0,0,1)→(2,0,2,1)
14.530	0.223	0.050	(0,0,0,0)→(2,0,2,0)
14.570	0.114	0.013	(0,0,0,0)→(2,1,1,0)
14.575	−0.171	0.029	(0,0,0,0)→(2,0,3,0)
14.598	−0.104	0.011	(0,0,0,0)→(3,0,0,0)
14.615	−0.115	0.013	(0,0,0,0)→(2,1,2,0)
14.621	0.104	0.011	(0,0,0,0)→(2,0,4,0)
14.643	0.157	0.025	(0,0,0,0)→(3,0,1,0)
14.688	−0.158	0.025	(0,0,0,0)→(3,0,2,0)
14.733	0.121	0.015	(0,0,0,0)→(3,0,3,0)

vibrational modes are excited in the photoionization to the D^2B_2 ionic state. This is opposite to the previous assignments [20–22], in which only contributions of the $\nu_3{}^+$ mode were considered. According to the current simulations, the first vibrational peak (marked with red arrow) is assuredly assigned to the $X^1A_1(0,0,0,0)\rightarrow D^2B_2(0,0,0,0)$ transition. Accordingly, the AIE of 14.125±0.005 eV is achieved and greatly agrees with the previous experimental results [20–22]. Moreover, the

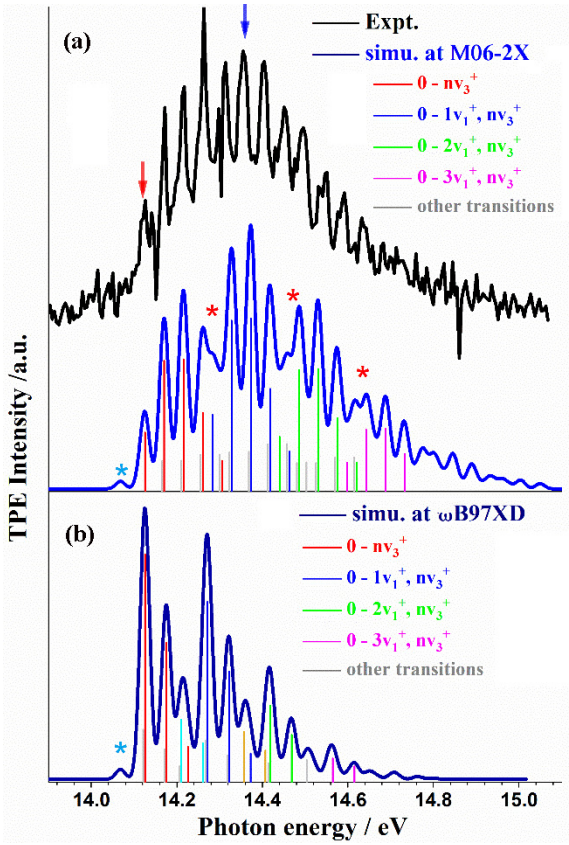

FIG. 3 Experimental and Franck-Condon simulated threshold photoelectron spectra of CF_2Cl_2 in the D^2B_2 ionic band, where the FWHM of 25 meV was used. The AIE and VIE are marked with red and blue arrows, respectively, and the hot-band is tabbed with blue star.

VIE of 14.355±0.005 eV for the D^2B_2 state is derived from the strongest vibrational peak in the simulated spectrum, which is marked with blue arrow in FIG. 3. The weak peak at the lowest energy side marked with blue star (14.067 eV) is attributed to the hot-band transition, $X^1A_1(0, 0, 1, 0)\rightarrow D^2B_2(0, 0, 0, 0)$.

Specifically, a few doublet peaks are theoretically expected and are marked with red stars in FIG. 3, however they are not observed in the experimental spectrum. For example, the calculated peaks of the $X^1A_1(0, 0, 0, 0)\rightarrow D^2B_2(0, 0, 3, 0)$ and $X^1A_1(0, 0, 0, 0)\rightarrow D^2B_2(1, 0, 0, 0)$ transitions should be discerned according to their energy difference of 0.023 eV, as indicated in Table V. However, only a single peak exists near this energy in the experimental spectra. Similar scenarios also arise at 14.485 eV and 14.643 eV (noted with red stars too in FIG. 3(a)). Moreover, the experimental vibrational peaks are systematically visibly red-shifted from the calculated ones above 14.3 eV. Hereby, we conjecture that this deviation might stem from the errors in the frequency calculations of different vibrational modes.

DOI: 10.1063/1674-0068/cjcp2308074

TABLE VI Assignments of the threshold photoelectron spectrum of CF_2Cl_2 towards the D^2B_2 state.

Peak	TPES		PES [21]	
	E/eV	$X^1A_1(\nu_{1-4})\rightarrow D^2B_2$ (ν_{1-4}^+)	E/eV	$X^1A_1(\nu_{1-4})\rightarrow D^2B_2(\nu_{1-4}^+)$
I	14.125	(0,0,0,0)→(0,0,0,0)	14.123	(0,0,0,0)→(0,0,0,0)
II	14.170	(0,0,0,0)→(0,0,1,0)	14.169	(0,0,0,0)→(0,0,1,0)
III	14.215	(0,0,0,0)→(0,0,2,0)	14.212	(0,0,0,0)→(0,0,2,0)
IV	14.260	(0,0,0,0)→(0,0,3,0) & (0,0,0,0)→(1,0,0,0)	14.459	(0,0,0,0)→(0,0,3,0)
V	14.315	(0,0,0,0)→(1,0,1,0)	14.307	(0,0,0,0)→(0,0,4,0)
VI	14.355	(0,0,0,0) → (1,0,2,0)	14.353	(0,0,0,0)→(0,0,5,0)
VII	14.405	(0,0,0,0)→(1,0,3,0) & (0,0,0,0)→(2,0,0,0)	14.399	(0,0,0,0)→(0,0,6,0)
VIII	14.450	(0,0,0,0)→(2,0,1,0)	14.447	(0,0,0,0)→(0,0,7,0)
IX	14.495	(0,0,0,0)→(2,0,2,0)	14.492	(0,0,0,0)→(0,0,8,0)
X	14.545	(0,0,0,0)→(2,0,3,0)	14.537	(0,0,0,0)→(0,0,9,0)
XI	14.590	(0,0,0,0)→(2,0,4,0) & (0,0,0,0)→(3,0,0,0)	14.582	(0,0,0,0)→(0,0,10,0)
XII	14.630	(0,0,0,0)→(3,0,1,0)	14.627	(0,0,0,0)→(0,0,11,0)

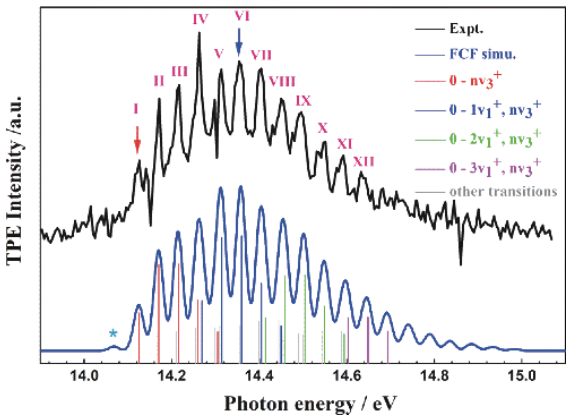

FIG. 4 Comparison between the experimental and Franck-Condon simulated threshold photoelectron spectra of CF_2Cl_2 in the D^2B_2 ionic band with the revised ν_1^+ frequency, where the FWHM of 25 meV was used.

To this end, we made a bold attempt that the vibrational frequency of ν_1^+ for the D^2B_2 state was modified from 1255 cm^{-1} to 1178 cm^{-1}. Using the calculated FCFs in Table V and the revised vibrational frequencies, we performed a new FC simulation for the experimental spectrum. The comparison between the experimental and new simulated spectra is shown in FIG. 4.

As shown in FIG. 4, the new simulated spectrum exhibits great agreement with the experimental one. Table VI lists the energy positions and corresponding assignments of the major twelve vibrational peaks in the D^2B_2 band, as well as the previous results obtained from the PES measurement of Jadrny *et al.* [21]. Notably, the present and previous spectral positions are greatly consistent, but their vibrational assignments are totally different above 14.3 eV. For instance, the peak at 14.355 eV is assigned to the $X^1A_1(0, 0, 0, 0)\rightarrow D^2B_2(1, 0, 2, 0)$ transition, while Jadrny *et al.* [21] attributed it to that of $X^1A_1(0, 0, 0, 0)\rightarrow D^2B_2(0, 0, 5, 0)$. Actually, the ν_1^+ and ν_3^+ frequencies are derived from the current simulations as 1178 cm^{-1} and 361 cm^{-1}, respectively (described below in detail). Notably, the ν_1^+ is about three times as large as ν_3^+, thus the fundamental excitation of ν_1^+ naturally overlaps with the overtone ν_3^+ excitation. Under this circumstance, the FCF simulation is an efficient approach to achieve accurate frequencies of these two vibrational modes.

Based on the above assignments, we can further evaluate anharmonic effects of the ν_1^+ and ν_3^+ vibrational modes. Using the vibrational transition series of $X^1A_1(0, 0, 0, 0)\rightarrow D^2B_2(m, 0, n, 0)$ ($m=0, 1, 2$. $n=0$–4) in Table VI, the harmonic vibrational frequencies (ω_e) of the ν_1^+ and ν_3^+ modes are achieved to be 1178 cm^{-1} and 361 cm^{-1}, respectively, according to the vibrational energy equation of $E_n = E_0 + \omega_e(n+1/2) - \omega_e\chi_e(n+1/2)^2$, where n is the vibrational quantum number. As shown in Table IV, these two frequencies perfectly agree with the calculated results and the previous values [18–22]. The anharmonic parameter for the ν_3^+ mode, $\omega_e\chi_e$, is determined to be 3.42 cm^{-1}. Compared with the value proposed by Pradeep *et al.* (0.27 cm^{-1}) [22], the current $\omega_e\chi_e$ value derived from the spectral simulation is obviously more reliable.

IV. CONCLUSION

In this work, we re-measured the TPES of CF_2Cl_2 in

DOI: 10.1063/1674-0068/cjcp2308074

the 11.60–15.10 eV photon energy range by applying TPEPICO approach. By calibrating the photon energies in the whole range with well-known absorption lines of argon gas, both AIE and VIE values of CF_2Cl_2 were corrected. Based on the upgraded AIE value of 11.590 eV and the AP (CF_2Cl^+/CF_2Cl_2) of 11.974 eV, the C–Cl bond energy of $CF_2Cl_2^+$ cation, BE (C–Cl in $CF_2Cl_2^+$), was determined to be 0.384 eV.

Specifically, the FCF simulations were performed for the D^2B_2 band of TPES of CF_2Cl_2, based on the optimized geometries and harmonic vibrational frequencies for the neutral CF_2Cl_2 and its cation in the D^2B_2 state, respectively, calculated at the ωB97XD and M06-2X levels with the aug-cc-pVTZ basis set. Although the two DFT methods showed generally consistent geometries, the simulated spectra patterns were significantly different, and the M06-2X/aug-cc-pVTZ results exhibited great agreement with the experimental vibrational structures. By comparing the simulated and experimental spectra, the vibrational assignments for the D^2B_2 band were achieved. Accordingly, the AIE and VIE towards the D^2B_2 state were determined as 14.125±0.005 eV and 14.355±0.005 eV, respectively. Moreover, vibrational frequencies of the ν_1^+ and ν_3^+ modes were 1178 cm^{-1} and 361 cm^{-1}, respectively.

In comparison to the previously reported ionization energy and vibrational frequencies, we have high confidence in the accuracy of current ionization energies and vibrational frequencies because of reliable spectral assignments.

V. ACKNOWLEDGEMENTS

The authors sincerely appreciate Prof. Qihe Zhu for continuous encouragement on photodissociation studies of small molecules. This work was financially supported by the National Natural Science Foundation of China (No.22073088 and No.22027801). Xiaoguo Zhou and Shilin Liu also thank the USTC-NSRL Association for financial support.

[1] B. J. Finlayson-Pitts and J. N. Pitts Jr., *Chemistry of the Upper and Lower Atmosphere: Theory, Experiments, and Applications*, San Diego, California: Elsevier, (1999).
[2] Y. Zhang, G. S. Oehrlein, E. de Frésart, and J. W. Corbett, J. Appl. Phys. **71**, 1936 (1992).
[3] D. J. Jacob, *Introduction to Atmospheric Chemistry*, Princeton, New Jersey: Princeton University Press, (1999).
[4] S. Solomon, Rev. Geophys. **37**, 275 (1999).
[5] D. G. Ralph and R. P. Wayne, J. Chem. Soc. Faraday Trans. 2 **78**, 1815 (1982).
[6] M. J. Molina and F. S. Rowland, Nature **249**, 810 (1974).
[7] H. W. Jochims, W. Lohr, and H. Baumgärtel, Ber. Bunsenges. Phys. Chem. **80**, 130 (1976).
[8] H. Schenk, H. Oertel, and H. Baumgärtel, Ber. Bunsenges. Phys. Chem. **83**, 683 (1979).
[9] J. M. Ajello, W. T. Huntress Jr., and P. Rayermann, J. Chem. Phys. **64**, 4746 (1976).
[10] X. K. Wu, G. Q. Tang, H. H. Zhang, X. G. Zhou, S. L. Liu, F. Y. Liu, L. S. Sheng, and B. Yan, Phys. Chem. Chem. Phys. **20**, 4917 (2018).
[11] D. P. Seccombe, R. P. Tuckett, and B. O. Fisher, J. Chem. Phys. **114**, 4074 (2001).
[12] Y. Chen, T. P. Yu, X. K. Wu, X. G. Zhou, S. L. Liu, F. Y. Liu, and X. H. Dai, Phys. Chem. Chem. Phys. **22**, 13808 (2020).
[13] X. K. Wu, X. G. Zhou, P. Hemberger, and A. Bodi, J. Chem. Phys. **153**, 054305 (2020).
[14] T. P. Yu, X. K. Wu, X. G. Zhou, A. Bodi, and P. Hemberger, Combust. Flame **222**, 123 (2020).
[15] X. K. Wu, X. G. Zhou, P. Hemberger, and A. Bodi, Phys. Chem. Chem. Phys. **22**, 2351 (2020).
[16] H. H. Zhang, T. P. Yu, X. K. Wu, Y. Chen, B. K. Shan, X. G. Zhou, X. H. Dai, and S. L. Liu, Chem. Phys. Lett. **774**, 138631 (2021).
[17] B. K. Shan, H. H. Zhang, T. P. Yu, Y. Chen, X. K. Wu, X. G. Zhou, and S. L. Liu, J. Mol. Spectrosc. **380**, 111506 (2021).
[18] J. C. Bunzli, D. C. Frost, F. G. Herring, and C. A. McDowell, J. Electron Spectrosc. Relat. Phenom. **9**, 289 (1976).
[19] D. W. Turner, A. D. Baker, C. Baker, and C. R. Brundle, Philos. Trans. Roy. Sot. London, Ser. A, Math. Phys. Sci. **268**, 7 (1970).
[20] T. Cvităs, H. Güsten, and L. Klasinc, J. Chem. Phys. **67**, 2687 (1977).
[21] R. Jadrny, L. Karlsson, L. Mattsson, and K. Siegbahn, Phys. Scr. **16**, 235 (1977).
[22] T. Pradeep and D. A. Shirley, J. Electron Spectrosc. Relat. Phenom. **66**, 125 (1993).
[23] X. F. Tang, X. G. Zhou, M. L. Niu, S. L. Liu, J. D. Sun, X. B. Shan, F. Y. Liu, and L. S. Sheng, Rev. Sci. Instrum. **80**, 113101 (2009).
[24] S. S. Wang, R. H. Kong, X. B. Shan, Y. W. Zhang, L. S. Sheng, Z. Y. Wang, L. Q. Hao, and S. K. Zhou, J. Synchrotron Radiat. **13**, 415 (2006).
[25] B. Sztáray and T. Baer, Rev. Sci. Instrum. **74**, 3763 (2003).
[26] X. K. Wu, X. F. Tang, X. G. Zhou, and S. L. Liu,

DOI: 10.1063/1674-0068/cjcp2308074

Chin. J. Chem. Phys. **32**, 11 (2019).
[27] A. Bodi, B. Sztaray, T. Baer, M. Johnson, and T. Gerber, Rev. Sci. Instrum. **78**, 084102 (2007).
[28] T. P. Yu, X. K. Wu, X. H. Ning, Y. Chen, X. G. Zhou, X. H. Dai, F. Y. Liu, and S. L. Liu, J. Phys. Chem. A **125**, 3316 (2021).
[29] X. K. Wu, X. G. Zhou, P. Hemberger, and A. Bodi, J. Phys. Chem. A **125**, 646 (2021).
[30] X. K. Wu, X. G. Zhou, S. Bjelic, P. Hemberger, and A. Bodi, J. Phys. Chem. A **125**, 3327 (2021).
[31] X. K. Wu, X. G. Zhou, S. Bjelić, P. Hemberger, B. Sztáray, and A. Bodi, Phys. Chem. Chem. Phys. **24**, 1437 (2022).
[32] Y. Zhao and D. G. Truhlar, Theor. Chem. Acc. **120**, 215 (2008).
[33] K. Takeshita, J. Mol. Spectrosc. **142**, 1 (1990).
[34] M. Lewerenz, B. Nestmann, P. J. Bruna, and S. D. Peyerimhoff, J. Mol. Struct.: THEOCHEM **123**, 329 (1985).
[35] T. Liu, M. B. Huang, and H. W. Xi, Chem. Phys. **332**, 277 (2007).
[36] J. D. Chai and M. Head-Gordon, Phys. Chem. Chem. Phys. **10**, 6615 (2008).
[37] V. A. Mozhayskiy and A. I. Krylov, ezSpectrum, http://iopenshell.usc.edu/downloads/.
[38] M. J. Frisch, G. W. Trucks, H. B. Schlegel, G. E. Scuseria, M. A. Robb, J. R. Cheeseman, G. Scalmani, V. Barone, G. A. Petersson, H. Nakatsuji, X. Li, M. Caricato, A. V. Marenich, J. Bloino, B. G. Janesko, R. Gomperts, B. Mennucci, H. P. Hratchian, J. V. Ortiz, A. F. Izmaylov, J. L. Sonnenberg, D. Williams-Young, F. Ding, F. Lipparini, F. Egidi, J. Goings, B. Peng, A. Petrone, T. Henderson, D. Ranasinghe, V. G. Zakrzewski, J. Gao, N. Rega, G. Zheng, W. Liang, M. Hada, M. Ehara, K. Toyota, R. Fukuda, J. Hasegawa, M. Ishida, T. Nakajima, Y. Honda, O. Kitao, H. Nakai, T. Vreven, K. Throssell, J. A. Montgomery Jr., J. E. Peralta, F. Ogliaro, M. J. Bearpark, J. J. Heyd, E. N. Brothers, K. N. Kudin, V. N. Staroverov, T. A. Keith, R. Kobayashi, J. Normand, K. Raghavachari, A. P. Rendell, J. C. Burant, S. S. Iyengar, J. Tomasi, M. Cossi, J. M. Millam, M. Klene, C. Adamo, R. Cammi, J. W. Ochterski, R. L. Martin, K. Morokuma, O. Farkas, J. B. Foresman, and D. J. Fox, *Gaussian 16, Revision C. 01*, Wallingford, CT: Gaussian Inc., (2016).
[39] A. Kramida, Yu. Ralchenko, J. Reader, and NIST ASD Team (2021). NIST Atomic Spectra Database (Ver. 5.9), [Online]. Available at https://physics.nist.gov/asd.

DOI: 10.1063/1674-0068/cjcp2308074